



UNIVERSITY OF LEEDS

This is a repository copy of *Geometric Variations of Modular Head-Stem Taper Junctions of Total Hip Replacements*.

White Rose Research Online URL for this paper:
<https://eprints.whiterose.ac.uk/164079/>

Version: Accepted Version

Article:

Wade, A, Beadling, AR orcid.org/0000-0001-5501-0140, Neville, A et al. (4 more authors) (2020) Geometric Variations of Modular Head-Stem Taper Junctions of Total Hip Replacements. *Medical Engineering & Physics*, 83. pp. 34-47. ISSN 1350-4533

<https://doi.org/10.1016/j.medengphy.2020.07.017>

© 2020 IPEM. Published by Elsevier Ltd. Licensed under the Creative Commons Attribution-NonCommercial-NoDerivatives 4.0 International License (<http://creativecommons.org/licenses/by-nc-nd/4.0/>).

Reuse

This article is distributed under the terms of the Creative Commons Attribution-NonCommercial-NoDerivatives (CC BY-NC-ND) licence. This licence only allows you to download this work and share it with others as long as you credit the authors, but you can't change the article in any way or use it commercially. More information and the full terms of the licence here: <https://creativecommons.org/licenses/>

Takedown

If you consider content in White Rose Research Online to be in breach of UK law, please notify us by emailing eprints@whiterose.ac.uk including the URL of the record and the reason for the withdrawal request.



eprints@whiterose.ac.uk
<https://eprints.whiterose.ac.uk/>

1 **Title**

2 Geometric Variations of Modular Head-Stem Taper Junctions of Total Hip Replacements

3 **Authors**

4 A. Wade^{a*}, A. R. Beadling^a, A. Neville^a, D. De Villiers^b, C. J. Cullum^b, S. Collins^b, and M. G. Bryant^a

5 ^a University of Leeds, School of Mechanical Engineering, Institute of Functional Surfaces, Leeds, UK;

6 ^b MatOrtho Ltd, Mole Business Park, Randalls Rd, Surrey, UK;

7 *Corresponding author, email: mn13aw@leeds.ac.uk

8 **Abstract**

9 Taper degradation in Total Hip Replacements (THR) has been identified as a clinical concern, and the
10 degradation occurring at these interfaces has received increased interest in recent years. Wear and
11 corrosion products produced at the taper junction are associated with adverse local tissue
12 responses, leading to early failure and revision surgery. Retrieval and in-vitro studies have found that
13 variations in taper design affect degradation. However, there is a lack of consistent understanding
14 within the literature of what makes a good taper interface. Previous studies assessed different
15 design variations using their global parameters assuming a perfect cone such as: taper length, cone
16 angle and diameters. This study assessed geometrical variations of as-manufactured head and stem
17 tapers and any local deviations from their geometry. The purpose of this study was to provide a
18 greater insight into possible engagement, a key performance influencing parameter predicted by
19 Morse taper connection theory. This was achieved by taking measurements of twelve different
20 commercially available male tapers and six female tapers using a coordinate measurement machine
21 (CMM). The results suggested that engagement is specific to a particular head-stem couple. This is
22 subject to both their micro-scale deviations, superimposed on their macro-scale differences.
23 Differences in cone angles between female and male tapers from the same manufacturer was found
24 to create a predominately proximal contact. However, distally mismatched couples are present in
25 some metal-on-metal head-stem couples. On a local scale, different deviation patterns were
26 observed from the geometry which appeared to be linked to the manufacturing process. Future
27 work will look at using this measurement methodology to fully characterise an optimal modular
28 taper junction for a THR prosthesis.

29 **Keywords/Phrases**

30 Taper, Geometry, Biotribocorrosion, Taper Interface, Modular Hip Prostheses

31 **1. Introduction**

32 Modularity of the femoral component in Total Hip Replacements (THR) is achieved by incorporating
33 a Morse-type taper at the head-stem connection ¹. It allows alternative head materials with varying
34 sizes and offsets to be used to balance soft tissues in order restore the natural gait ^{2,3}. Modularity
35 also offers the ability to retain well fixed femoral stems while replacing the femoral head reducing
36 the risk of morbidity, bone loss and soft tissue damage during revision surgery ⁴. Exchanging the
37 femoral head while retaining the stem during revision surgery has been recorded to occur in around
38 45 % of primary revision surgeries in Sweden, according to the Swedish Joint Registry ⁵. The 15th
39 annual joint registry for England, Wales, Northern Ireland and Isle of Man (NJR) ⁶ indicates that at
40 least 630,000 THR implanted between 2003 and 2017 included head-stem modularity. However,
41 moving from a mono-block to a modular design has meant fluid ingress and micro-motion at the
42 interface, leading to a complex degradation mechanism between fretting and corrosion (i.e. fretting-
43 corrosion) ⁷⁻⁹. Gilbert et al. ⁸ investigated degradation due to head-stem modularity coining the term
44 Mechanically Assisted Crevice Corrosion (MACC) to describe the mechanical and chemical
45 degradation mechanisms and any interdependence they may have. Wear and corrosion products at
46 the taper junction are associated with adverse local tissue reactions commonly presented in patients
47 as pain followed by instability ¹⁰⁻¹³. Fretting-corrosion at the head-stem junction can also present
48 systemic implications, and in some cases go on to cause catastrophic implant failure such as neck
49 fracture or head dislocation due to excessive material loss ^{2,11,14,15}. The NJR ⁶ found that of all primary
50 hip replacements, 2.8 % required revision and of that, 17 % were due to adverse soft tissue reaction
51 to particle debris; where the head-stem taper junction is a possible generation source. Taper
52 degradation is a clinical concern and has been received increasing interest in recent years ^{11,15-17}.
53 This was highlighted by a recent retrieval study conducted by Ridon et al. ¹⁸ that compared matched
54 cohorts of metal-on-metal (MoM) THR with resurfacing (no modular femoral stem). They found that
55 almost 30 % of the THR cohort underwent revision due to adverse reactions to metal debris
56 compared to 0 % for the resurfacing cohort, highlighting that the head-stem interface would appear
57 to be a prominent interface for metal ion release. Whilst there has been a dramatic decrease in the
58 use of MoM THR, which now make up only around 4 % of implanted, taper degradation is still a
59 clinical concern with evidence of degradation occurring in all bearing combinations ^{6,13,16,17,19,20}.

60 Morse tapers were originally designed to allow machine parts such as drill bits and cutting tools in
61 milling machines to be changed quickly without compromising torque transmission ¹. This is
62 achieved by an interference fit between male and female conical surfaces allowing torque
63 transmission under a simple compressive force along the taper length. The original Morse taper
64 achieved a sufficient interference fit by designing the two interfaces to be highly conforming,

65 smooth, hard (usually case-hardened steel), long and with a slight taper angle ²¹⁻²³. These design
66 features provide a sufficient compressive fit over the whole mating taper surface to resist shear
67 stress from applied torque. Hardening is undertaken for a number of reasons including: to increase
68 cylindrical accuracy, stiffness and to reduce damage due to handling and fretting from mismatched
69 mating surfaces. Absolute conformity is hard to achieve and so tapers have commonly been
70 designed to relieve the contact at the centre, for a good fit without shaking due to contact at either
71 end ²². It was also originally advised not to impact tapers, but to use a press to ensure alignment and
72 equal strain or distortion for use in lathes ²¹.

73 Head-stem tapers used in THR on the other hand are much shorter with a higher taper rate (i.e.
74 shorter with a greater taper angle), often presenting a threaded finish and a level of angular
75 mismatch (i.e. the difference in cone angle between the female and male taper, see Figure 1) in
76 order to create specific contact regions ^{1,24}. Additionally, the biomechanical loading profile of the
77 head-stem taper in-vivo is complex with a cyclic nature, very different from that experienced in
78 Morse tapers ²⁵. Morse tapers were designed to transmit high torques under a dominant
79 compressive axial load (i.e. two axes) ¹. The sort of mechanical loads experienced at the taper
80 junction are complex and include loading in six axes ^{26,27}. These are dynamic loads and can exceed
81 body weight by almost a factor of four ²⁵. The complex biomechanical loading facilitates micro-
82 motions and fluid ingress with abundant electrochemically active species for fretting-corrosion ⁸.
83 Degradation of the taper junction in THR has been found to vary with different design parameters
84 including: surface roughness, diameters, angular mismatch, length and flexural rigidity ^{9,28-35}.
85 However, links to clinical performance are often limited to high level descriptions such as short and
86 rough or long and smooth ^{32,36}.

87 Engagement of the two conical surfaces has been historically determined by differences in the
88 geometrical form of the male and female taper assuming an ideal cone and deviations from that
89 geometry. This is usually parametrised by angular mismatch, taper length and surface roughness
90 (see Figure 1) ^{31,33-35,37,38}. However, just looking at the geometry assuming an ideal cone and surface
91 topography provides limited insight into possible engagement for further performance assessment.
92 Witt et al. ³⁹, investigated the engagement of unique head-stem couples by using a gold coating on
93 the male taper, quantifying the removal of this film upon engagement. It was found that
94 engagement of the two surfaces was inconsistently distributed. This raises questions about the
95 conformity of the interface and/or about the impaction process being self-aligning even under
96 quasi-static loading.

97 This study assessed geometrical variations of as-manufactured head and stem tapers and any local
 98 deviations from their geometry, giving a greater insight into possible engagement. Outputs from this
 99 study will be used in future work to allow a more descriptive link between taper design and clinical
 100 performance. This was achieved by taking precise geometric measurements of clinically available
 101 male and female tapers using a coordinate measurement machine (CMM) with development of
 102 bespoke analysis algorithms.

103 **2. Materials and Methods**

104 Measurements were taken using a coordinate measurement machine (CMM, Legex 322, Mitutoyo,
 105 Japan) accurate to 0.28 µm. The study included twelve different commercially available male tapers
 106 and six female tapers (see Table 1). Two of the ten male tapers (MT4 and MT5) were manufactured
 107 from simplified spigot coupons, while all the others were full femoral stem. This meant that MT4
 108 and MT5 were clinical '12/14' tapers manufactured from 14 mm diameter bar stock. Manufacturer
 109 and product information was kept anonymous for commercial reasons.

110 *Table 1 Details of samples measured using CMM, where 'n' corresponds to the number of different samples. NB 'Spigot'*
 111 *indicates a spigot coupon as opposed to a full stem and rough indicates a visibly 'threaded' type finish.*

Male Taper (MT)/Female Taper (FT)	Manufacturer	Type	Rough (Yes/No)	Collared (Yes/No)	Material	n
MT 1	A	12/14	Yes	Yes	CoCrMo	2
MT 2	A	12/14	Yes	No	CoCrMo	3
MT 3	A	12/14	Yes	No	Ti6Al7Nb	1
MT 4	B	12/14 Spigot	Yes	No	CoCrMo	3
MT 5	B	12/14 Spigot	Yes	No	Titanium Alloy	6
MT 6	B	12/14	Yes	No	CoCrMo	1
MT 7	C	12/14	Yes	No	Stainless Steel	8
MT 8	C	10/12	No	No	CoCrMo	8
MT 9	D	12/14	No	No	CoCrMo	1
MT 10	E	Type 1	No	Yes	CoCrMo	1
MT 11	C	12/14	Yes	No	Titanium Alloy	3
MT 12	C	12/14	Yes	Yes	Titanium Alloy	3
FT 1	A	12/14	-	-	CoCrMo	1
FT 2	A	12/14	-	-	CoCrMo	1
FT 3	B	12/14	-	-	CoCrMo	2
FT 4	B	12/14	-	-	Zirconia Toughened Aluminium Oxide	1
FT 5	C	12/14	-	-	CoCrMo	4
FT 6	C	12/14	-	-	CoCrMo	2

112
 113 The taper surface was scanned using a 1.5 mm diameter ruby with stylus that was 30 mm long. The
 114 same measurement strategy was used for both male and female tapers. The flat proximal end of the
 115 tapers was used to create the x-y plane in which the origin lay at the centre, as shown in Figure 1a
 116 and b. The traces consisted of 32 equally spaced vertical traces along the length of the longitudinal
 117 axis of the taper (z-axis) and circumferential traces at 0.5 mm spacing, as shown in Figure 1 c and d.
 118 Although each trace was taken as a continuous contour, a pitch of 0.1 mm was used. The

119 circumferential spacing was selected based on being half the recommended spacing between traces
 120 when measuring wear of total hip prostheses according to ISO 14242-2⁴⁰. Thirty-two equally spaced
 121 vertical traces was selected as this demonstrated convergence of the calculated taper angle with
 122 that calculated using the horizontal traces.

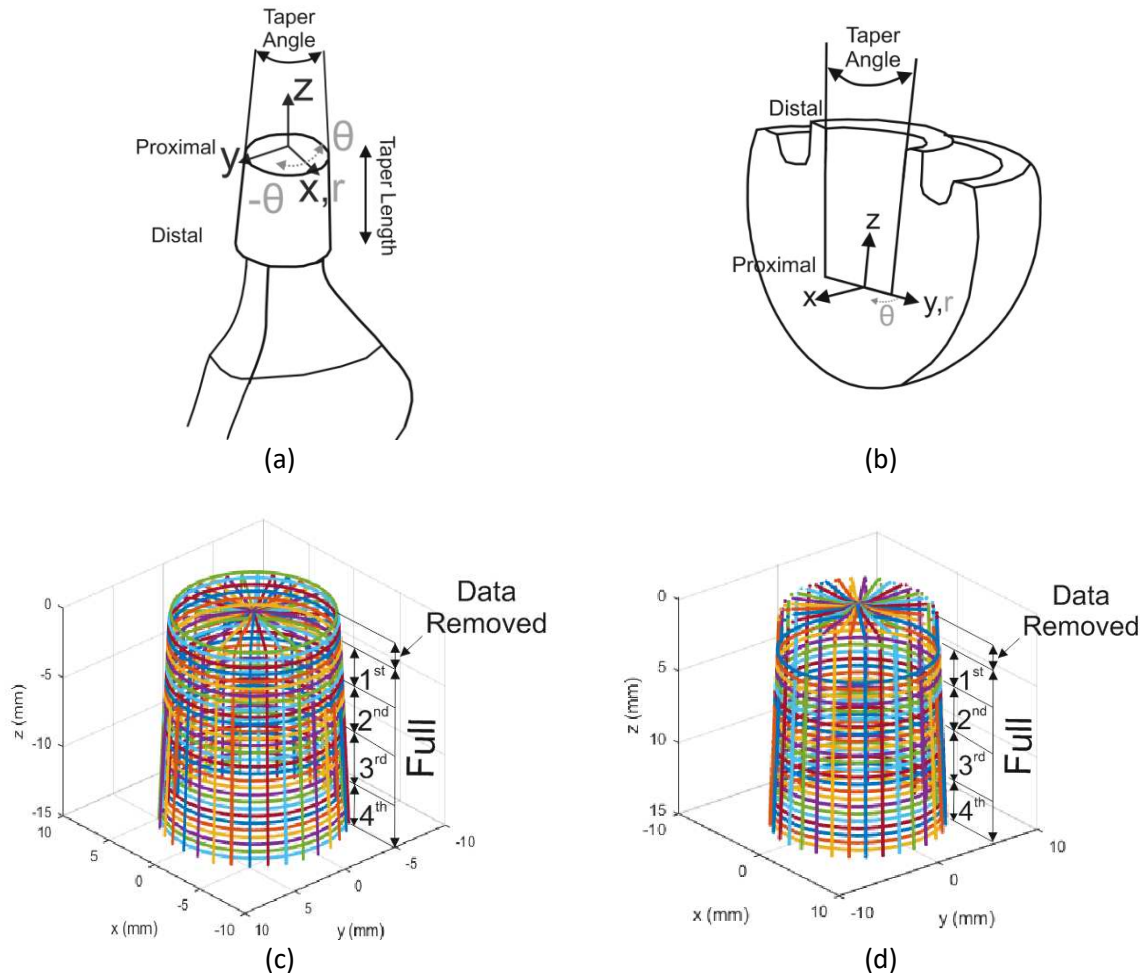


Figure 1 Schematic of the CMM cartesian (black) and cylindrical polar (grey) coordinate systems with respect to the (a) male taper stem geometry and (b) female taper head geometry. Vertical and circumferential scans on a (c) male taper and (d) female taper. Annotations indicate the data removed for analysis and the quarter cone analysis using the vertical scans (i.e. '1st', '2nd', '3rd' and '4th') and full length of the taper (i.e. 'full').

123 The raw data was exported in 3D cartesian coordinates to allow bespoke analysis using MatLab
 124 (R2017a, MathWorks, USA). Stems were aligned with the coordinate systems as shown in Figure 1a
 125 by using the symmetry of the stems in a vice and engineering parallels to minimise the amount of
 126 rotation about the z-axis between stem measurements.

127 Prior to any analysis, the chamfer of the male taper and the proximal clearance area of the female
 128 taper was removed from all the data sets. This was achieved by excluding data from the first 1.5 mm
 129 of the male tapers (i.e. from $z = 0$ to $z = -1.5$ mm) and the first 2 mm of the female taper (i.e. $z = 0$
 130 mm to $z = 2$ mm, Figure 1 c and d). Taper angle (or cone angle) was then calculated independent of
 131 any rotation about the x and y axes by using two directly adjacent vertical traces and applying the

132 cosine rule. This was done using both the full length of the taper and by segmenting it into quarters
 133 as shown in Figure 1 c and d. The first step was to apply a linear regression to each segment to find
 134 the relationship between the x, y and z coordinates. These were then used to determine the vector
 135 equation of each segment before applying the cosine rule to the directly opposite corresponding
 136 segment vector (see Figure 1 c and d). This was repeated and averaged over the sixteen different
 137 planes about the taper axis i.e. using two vertical scans located on direct opposite sides of the taper
 138 for a single plane.

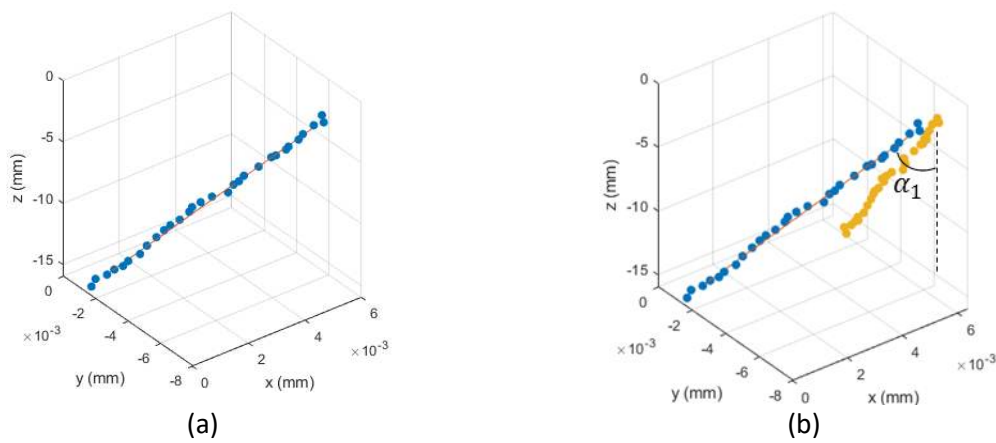
139 Circumferential traces were used to determine deviation from the ideal cone. Tilt about the x and y
 140 axes was removed prior to analysis. This was achieved by first finding the relationship between x, y
 141 and z coordinates of the centres of each circumferential traces (Figure 2a). Two angles were then
 142 calculated from this linear relationship: 1) between the y-z plane and the component of the linear
 143 relationship in the x-z plane (α_1 , Figure 2b) and 2) between the x-z plane and the component of the
 144 linear relationship in the y-z plane (α_2 , Figure 2c). These angles were then used to create two
 145 rotation matrices for rotation about the y-axis ($T_{\text{rot } y(\alpha_1)}$, Equation 1) and x-axis ($T_{\text{rot } x(\alpha_2)}$, Equation
 146 2).

$$T_{\text{rot } y(\alpha_1)} = \begin{bmatrix} \cos(\alpha_1) & 0 & \sin(\alpha_1) \\ 0 & 1 & 0 \\ -\sin(\alpha_1) & 0 & \cos(\alpha_1) \end{bmatrix} \quad \text{Equation 1}$$

$$T_{\text{rot } x(\alpha_2)} = \begin{bmatrix} 1 & 0 & 0 \\ 0 & \cos(\alpha_2) & -\sin(\alpha_2) \\ 0 & \sin(\alpha_2) & \cos(\alpha_2) \end{bmatrix} \quad \text{Equation 2}$$

147

148 After rotating all the points from the circumferential traces it was then translated to centre all the
 149 data about the origin (Figure 2d).



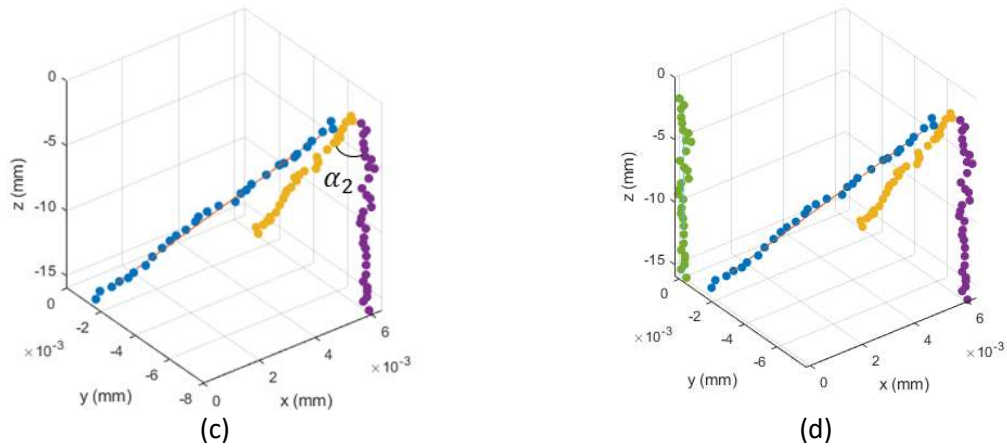


Figure 2 (a) Centres of each circumferential trace and 3D linear regression (b) rotation about the y-axis i.e. in the x-z plane (c) rotation about the x-axis i.e. in the y-z plane and (d) translation about the origin.

150 Ideal taper angle was calculated by converting to a cylindrical polar coordinate system (Figure 1a and
 151 b). Cone angle was determined by taking tangent of the gradient coefficient of the linear relationship
 152 between radii (r) and the z-axis. The full taper length was used as the cone generator (i.e. equation
 153 of the line of best fit that relates radius to the z position along the taper) for determining deviation
 154 from the ideal cone. Still within cylindrical polar coordinates, the ideal cone radii at any given z-value
 155 was calculated from the cone generator and taken from the radial position (r) of each point.
 156 Deviation was then plotted as a surface plot against position around the taper (θ) and the z-axis of
 157 the taper.

158 Taper angles and deviation from the cone was also verified with a predeveloped cone analysis
 159 software (Sphere Profiler, Redlux, UK). There was less than a 0.0001° discrepancy in cone angle
 160 between the bespoke MatLab analysis and the predeveloped geometry analysis software with
 161 matching deviation patterns (Figure 3).

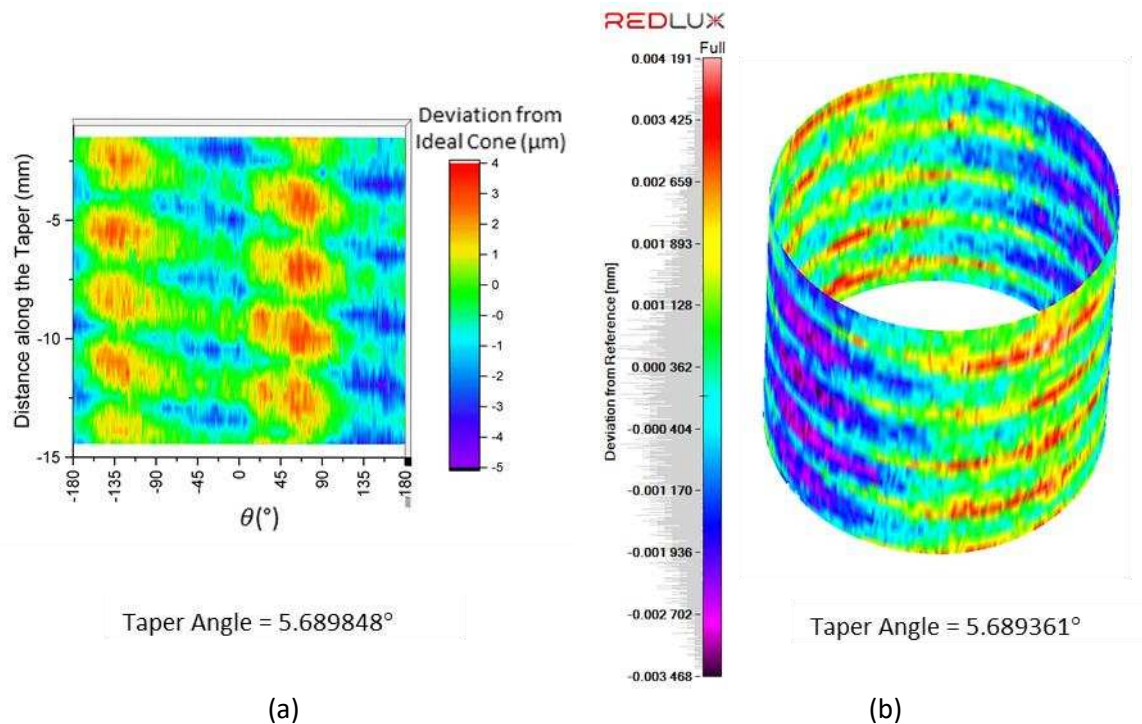


Figure 3 Example of a taper analysed using the (a) bespoke MatLab programme and (b) predeveloped Redlux analysis which shows similar taper angles and deviation patterns.

162 **2.1. Statistics**

163 Data is presented as a mean \pm 95 % confidence intervals unless stated otherwise. Taper angles were
 164 compared using 1-way analysis of variance followed by the students t-test. Level of significance was
 165 set at p-value of 0.05 for all statistical tests. The statistical analyses were performed using Excel
 166 (Microsoft, USA).

167 **3. Results**

168 **3.1. Taper Angle**

169 Figure 4 shows the calculated male taper angles. These varied between male tapers, even those of
 170 the apparent same type i.e. the '12/14' male tapers (P-value <0.05). Statistical difference was seen
 171 between the majority of the male tapers, including those of the same type and manufacturer e.g.
 172 MT7 and MT11 with MT12. The '12/14' male tapers demonstrated an average taper angle of $5.659 \pm$
 173 0.0131° and range of 0.08° , shown in Figure 4a. MT8 ('10/12' taper) and MT10 (Type 1 taper)
 174 demonstrated a significantly reduced average angle of 3.070° and 3.773° respectively (Figure 4b
 175 and c). Figure 4 displays the cone angles and confidence intervals from repeats on separate samples
 176 of the same type and the 16 different planes about the z-axis providing an indication of "roundness".
 177 The smallest confidence intervals belong to spigots (MT4 and MT5) and, MT7.

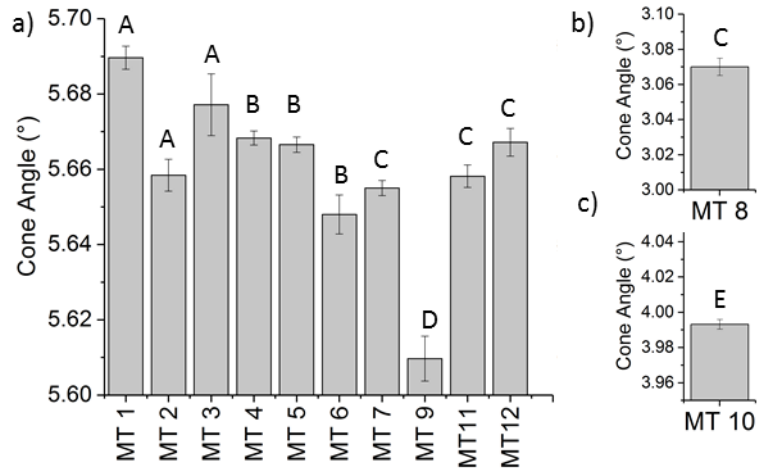


Figure 4 Taper angles of (a) '12/14' male tapers and (b) '10/12' (MT8) and (c) Type 1 (MT10). Letters above each bar indicates the manufacturer (see Table 1). Error bars correspond to the 95 % confidence intervals from the taper angles calculated using the sixteen equally spaced different cones about the z-axis. NB although the scales are very different the range are a consistent 0.1° for comparison.

178 The female taper angles, all of which are '12/14', were different (p-value <0.05) except FT2 and FT4
 179 (Figure 5). The female tapers demonstrated an average larger cone angle of $5.712 \pm 0.043^\circ$ and
 180 range of 0.13° compared to the '12/14' male tapers, providing a predominantly proximal contact
 181 between ideal cones. However, FT5 and FT6 from manufacturer C presented a much smaller taper
 182 angle. The female tapers presented a similar taper angle variation between tapers of the same type
 183 as the male tapers reflected by the confidence intervals in Figure 4 and Figure 5.

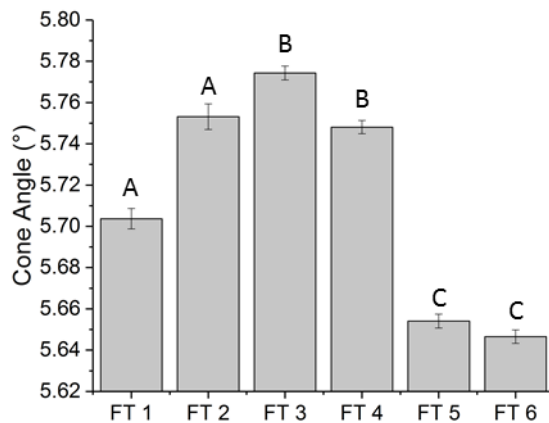


Figure 5 Taper angles of all female tapers. Letters above each bar indicates the manufacturer (see Table 1). Error bars correspond to the 95% confidence intervals from the taper angles calculated using the sixteen equally spaced different cones about the z-axis.

184 Variation in cone angle also occurred along the length of the taper providing an indication
 185 as to 'straightness'. Figure 6 shows cone angle calculated from the male tapers
 186 segmented into quarters. There appeared to be no consistent variation pattern between the tapers
 187 but there was statistical difference between the quarters in most of the male taper apart from MT3
 188 and MT7. MT10 demonstrated the largest variation in cone angle down the taper with a maximum

189 difference of 0.169 ° between the quarters. The smallest variation was seen by the MT7 with a
 190 difference of 0.003 °.

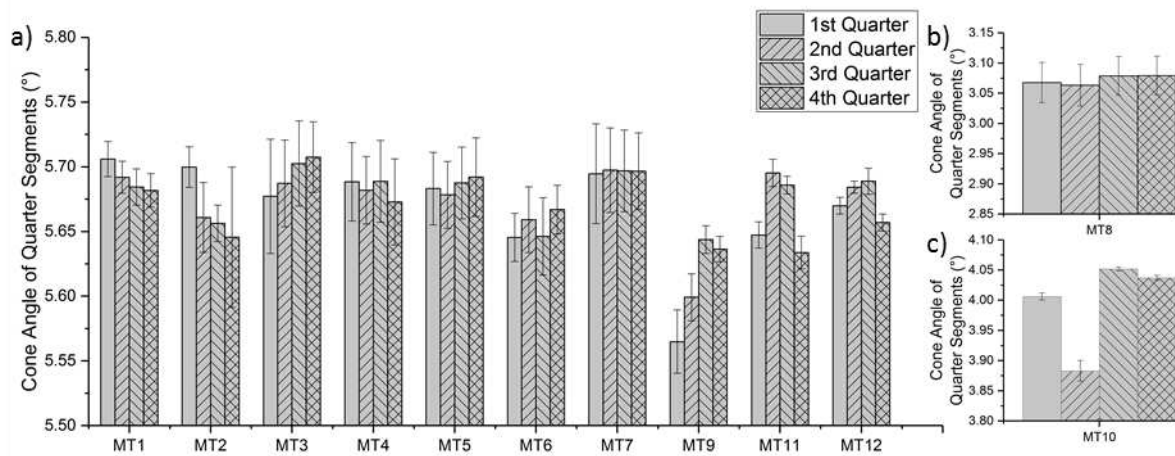


Figure 6 Male taper angles segmented into quarters where the 1st quarter corresponds to the most proximal and the 4th quarter corresponds to the most distal. (a) '12/14' male tapers and (b) the '10/12' (MT8) and (c) Type 1 taper (MT10). NB although the scales are very different the range are a consistent 0.3 ° for comparison.

191 Taper angle variation along the length was also seen in the female tapers, as shown in Figure 7.
 192 Similar variation in cone angle was seen in the different quarters between the male and female
 193 tapers. Variation between the quarters were all significantly different.

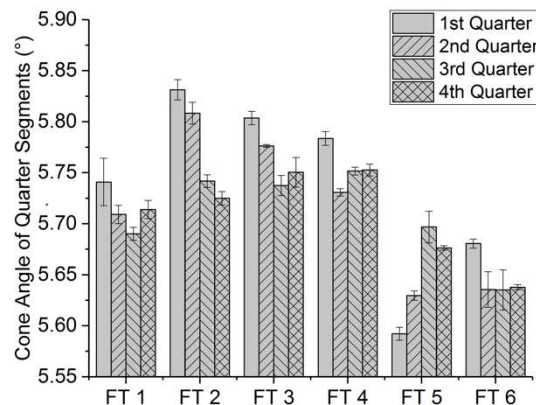


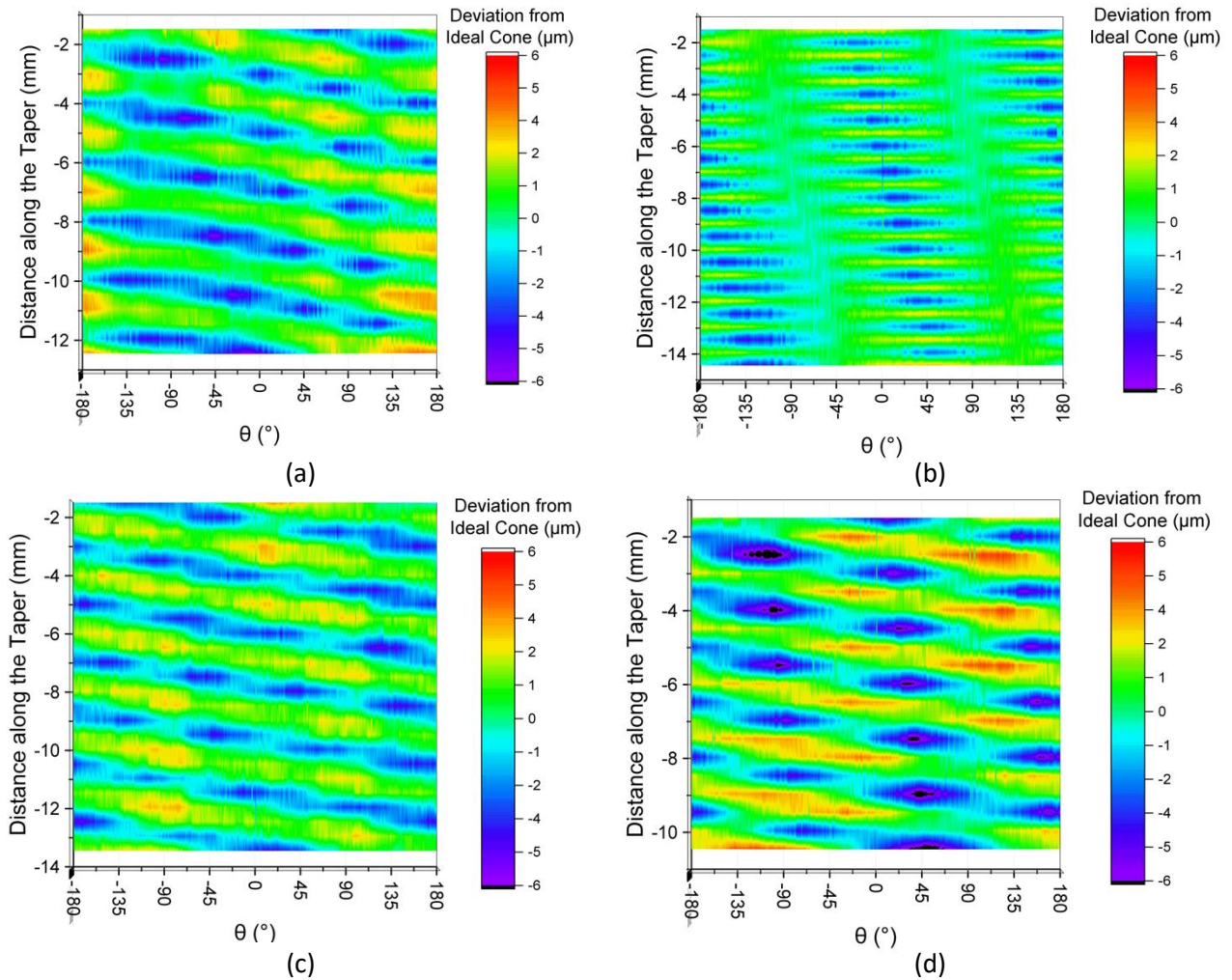
Figure 7 Female taper angles segmented into quarters where the 1st quarter corresponds to the most proximal and the 4th quarter corresponds to the most distal.

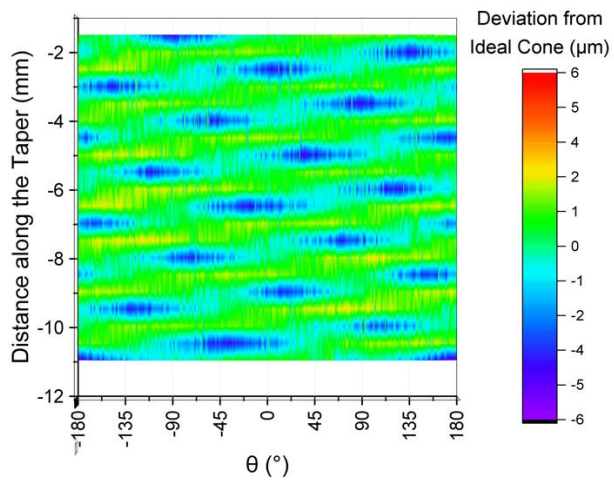
194 3.2. Deviation from the Ideal Cone

195 3.2.1. Male Tapers

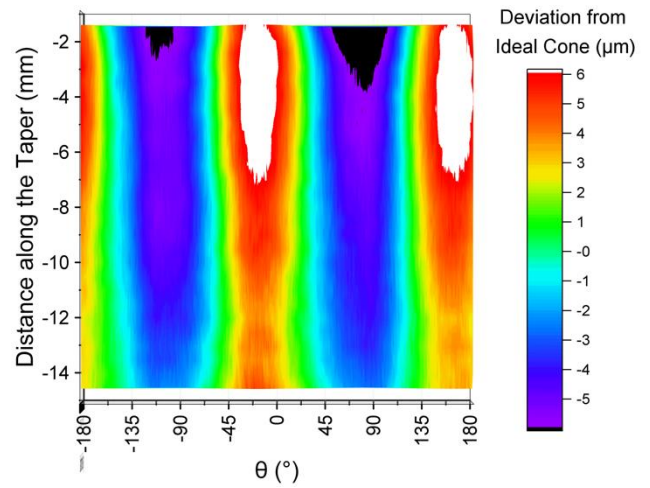
196 The variation in taper angle around and along the z-axis of the taper (i.e. 'roundness' and
 197 'straightness') are due to deviations from the ideal cone. Figure 8 shows surface deviation patterns
 198 for the male tapers. In cases where there was more than one sample per taper for measurement,
 199 the same deviation pattern was observed. Clear 'threaded' patterns were seen in: MT3, the spigots
 200 (MT4 and MT5), MT6, MT7 and MT12 (Figure 8a, b, c, d and e respectively). The largest pitch of
 201 0.286 mm was measured on MT7, using simple circle geometry a pitch of 0.286 mm would allow a

202 1.5 mm diameter ruby a circle sagitta of 0.0136 mm. corresponding with great precision to the CMM
 203 deviation range of the ideal cone of 0.0136 mm. Out of “roundness” in the form of ovality
 204 demonstrated by a two sine waves equally distributed around the taper was seen in MT8 and MT10
 205 (Figure 8f and g respectively). MT1, MT2 and MT11 demonstrated a deviation pattern characteristic
 206 of a ‘threaded’ taper with ovality (Figure 8h, i and j respectively). MT9 presented the smallest
 207 deviation range of 0.0035 mm (less than 40 % of the average deviation range of all the male tapers)
 208 with a pattern that indicated that there might have been ideal cone fitting mismatch (Figure 8k). The
 209 location of the major and minor axes of ovality were distributed at the same location relative to the
 210 stem geometry for the MT8, MT2 and MT11 tapers. The major axis occurred at approximately $\theta = 0^\circ$
 211 and $\theta = \pm 180^\circ$ (in cylindrical polar coordinates) corresponding the plane of them stem that would
 212 allow provide the smallest second moment of area as shown in Figure 1a. The collared MT1 and
 213 MT10 presented an oval pattern that was out of phase with MT2 and MT8 (both of which are non-
 214 collared) by around 60° .

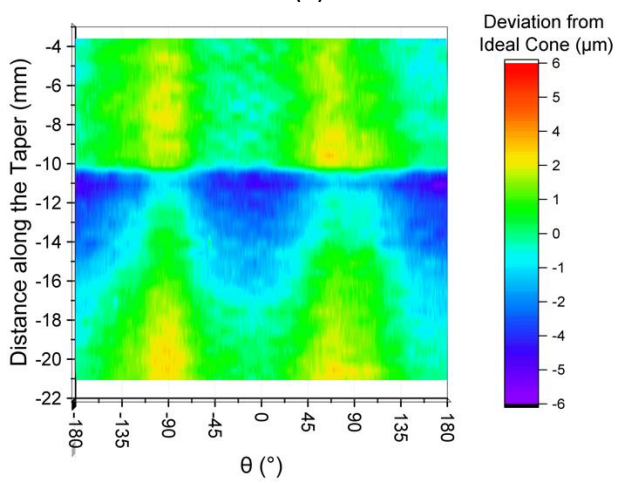




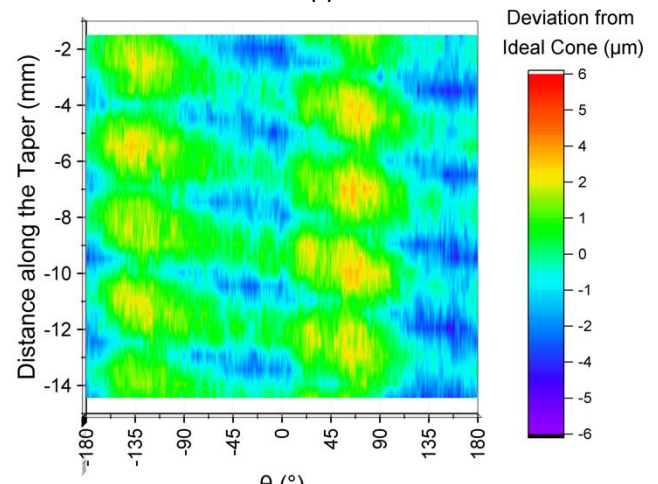
(e)



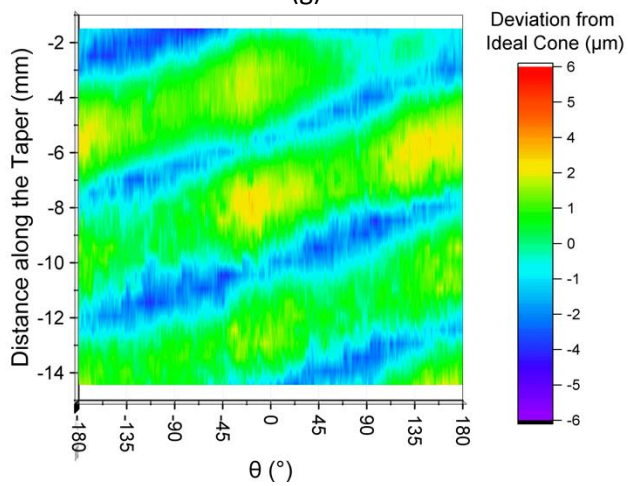
(f)



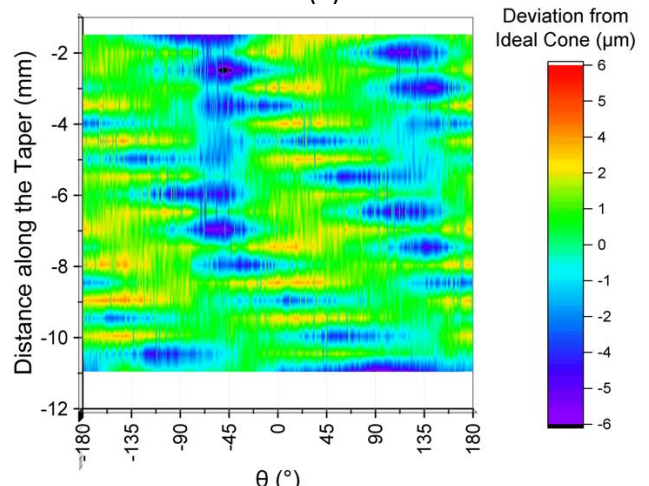
(g)



(h)



(i)



(j)

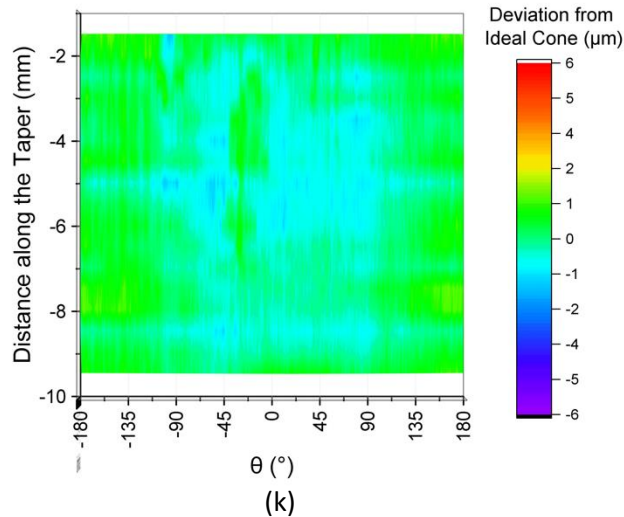
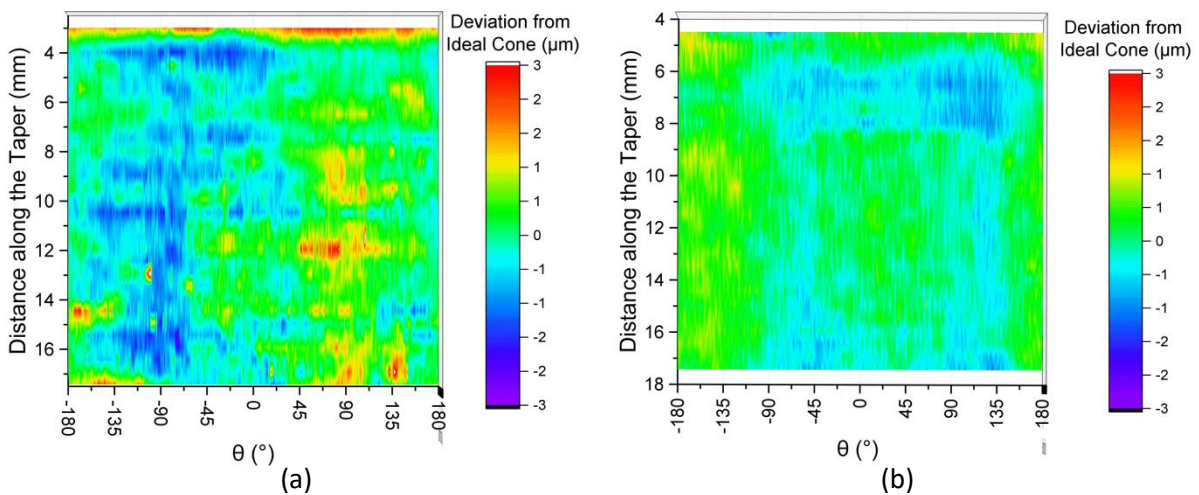


Figure 8 Surface maps of the deviation from the ideal cone in cylindrical polar coordinates for male tapers. (a) MT3 (b) MT4 (c) MT6 (d) MT7 (e) MT12 (f) MT8 (g) MT10 (h) MT1 (i) MT2 (j) MT11 (k) MT9.

215 3.2.2. Female Tapers

216 The female and male tapers presented a similar range of deviation (10 μm vs 9 μm for male and
 217 female tapers respectively) but very different deviation patterns. In cases where there was more
 218 than one sample of the same taper for measurement, the same deviation pattern was observed.
 219 Figure 9 shows the deviation maps from the ideal cone for all the female tapers. Three different
 220 patterns were observed in the female tapers. FT1 and the ceramic FT4 tapers presented no
 221 repeating patterns around the taper z-axis or along it (Figure 9a and b). No repeating patterns were
 222 presented in FT1 and FT4 indicate eccentricity that could be a function of ideal cone fitting
 223 mismatch. The ceramic taper (FT4) demonstrated the smallest deviation range, around 40 % smaller
 224 than other female tapers. The four remaining female tapers presented a third order harmonic
 225 around the z-axis of the taper including: FT2, FT3, FT 5 and FT 6 (Figure 9c, d, e and f). It was noted
 226 that the four female tapers that presented this triple harmonic belonged to all the solid metal heads
 227 in this study. FT2 was the only other CoCrMo head in this study did not present this pattern and was
 228 of a separate bearing surface and taper insert (i.e. hollow).



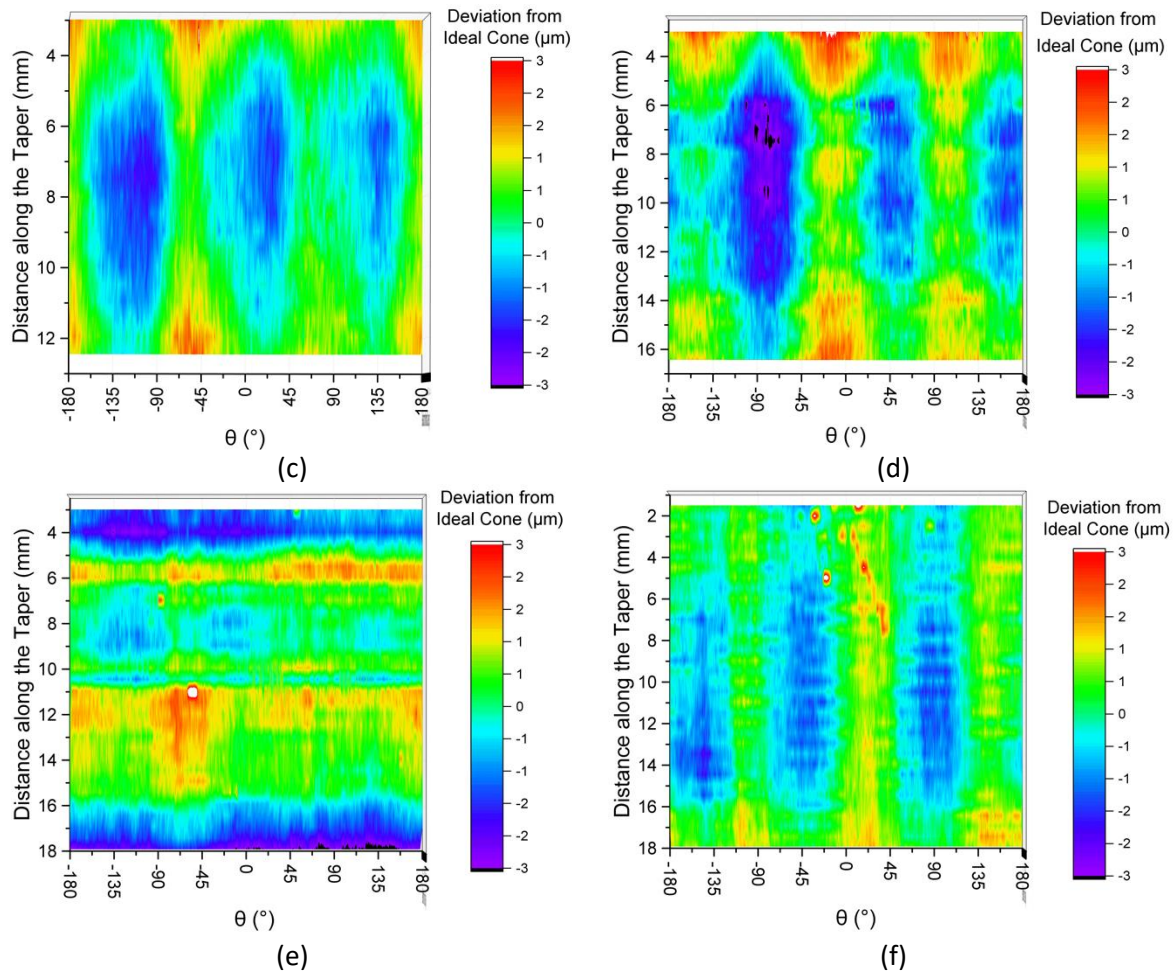


Figure 9 Surface maps of the deviation from the ideal cone in cylindrical polar coordinates for female tapers. (a) FT1, (b) FT4, (c) FT2, (d) FT3, (e) FT5 and (f) FT6.

229 4. Discussion

230 The aim of this study was to assess variations in commercially available male and female THR head
 231 and stem tapers providing a greater insight into possible engagement. The largest limitation in
 232 assessing variation across the market came from the number of repeat samples for each taper.
 233 Although an aim of a minimum of three samples per taper measured, this was not always possible.
 234 The limited number of samples should be taken into account when drawing conclusions from this
 235 study, especially where only one was available for measurement. Another limitation of this study
 236 was the use of a contacting CMM with a 1.5 mm diameter ruby tipped stylus. This introduced a
 237 degree of mechanical filtering of the surfaces which meant that finer surface topographical
 238 characteristics such as machining marks were not accurately captured.

239 One of the first observations of this study was that tapers of the apparent same type (i.e. '12/14')
 240 presented different ideal geometries. Variation in the '12/14' male taper cone angles varied by a
 241 range of 0.08° (Figure 4a). While the '12/14' female taper cone angle varied by a range of 0.13°
 242 (Figure 5). Both male and female cone angle variation ranges agreed with Mueller et al.³⁷ that

243 reported a variation of about 0.1 ° between manufacturers. Likewise, MT10 presented a smaller
244 cone angle than the '12/14' tapers and within the range given by Nassif et al. ⁴¹. The '10/12' taper
245 (MT8) presented the smallest cone angle, closer to that intended by Morse to resist shear stresses ¹.
246 Smaller taper angles would decrease the taper locking stiffness allowing a greater displacement
247 under the same impaction loads, increasing seating energy as explained by Ouellette et al. ⁴².
248 However, it is unclear how taper angle might affect performance of the junction under biological
249 loading condition and if Morse's original design criteria of only a slight taper is beneficial.

250 Taper angle was affected by 'roundness' and 'straightness'. Variation in the cone angle within the
251 different planes about the z-axis of the taper provided a good indication of out of 'roundness'. While
252 differences between the cone angles once split into quarters gave an indication as to the
253 'straightness' of the conical tapers. This effect of 'straightness' was seen directly in The Type 1 taper
254 (MT10) that demonstrated the largest maximum and minimum cone angles calculated from splitting
255 the taper into quarters. This was predominantly due to variation seen in the 2nd quarter (Figure 6c),
256 corresponding to the large step seen in the deviation from the cone maps at around z= -11 mm
257 (Figure 8g).

258 Assuming an ideal geometry, deviations in 'straightness' and 'roundness' present uniquely different
259 patterns between female and male tapers. Therefore, this study suggests that engagement of a
260 taper junction in modular head-stem THR is not as simple as that predicted by angular mismatch of
261 the ideal geometries. Rather, engagement or contact area is specific to a particular head-stem
262 couple subject to differences in geometrical form with a waviness and roughness that will result in a
263 stochastic contact. In regions of sufficient compressive stress these contacting asperities will
264 experience deformation altering the as-manufactured surfaces ³⁹. Further changes to the surface will
265 also arise from fretting-corrosion, constantly wearing and corroding the contacting asperities leading
266 to a transient interface changing with time in situ ⁴³. Studies have identified that wear and corrosion
267 at the interface is enhanced with a decrease in conformity in terms of a 'rough' male taper, shorter
268 engagement lengths and other features that reduce conformity such as the 'scalloped' regions
269 present in SROM stems ^{29,32,36}. The patterns observed in this study will have an implication on
270 conformity at this interface and actual contact area, as was reported by Jones et al. ⁴² that found
271 different contact area distributions that support the 'roundness' and 'straightness' patterns
272 observed in this study. Future work is aimed at mapping out a link between taper design and
273 performance in terms of this highly transient interface. This will help understand if these variations
274 seen in this paper are significant to performance over time and ultimately to their clinical
275 performance.

276 This study found that both male and female taper angles presented differences, not only between
 277 manufacturers, but between products with the same taper type and of the same manufacturer.
 278 Taper angle is arguably the most important manufacturing tolerance to ensure a tight uniform fit
 279 between male and female tapered surfaces. The most applicable standards for tolerances are
 280 detailed by ISO 1947⁴⁴ which describes twelve different taper angle tolerance grades from AT1 to
 281 AT12. For cones of between 10-16 mm length the tightest tolerance grade (AT1) prescribes a
 282 maximum variance of 10'' (0.003 °) in cone angle (AT_α , see Figure 10) and 0.4-0.6 μm between the
 283 largest and smallest diameter (AT_D) at the end of the cone (L). At the same taper length the loosest
 284 tolerance grade (AT12) prescribes maximum variances of 21'38'' (0.36 °) in cone angle and 63-100
 285 μm difference in diameter at L.

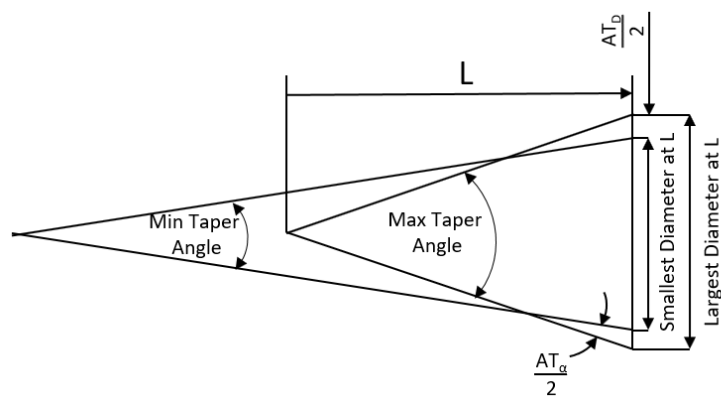


Figure 10 Schematic of the relevant taper tolerances described in ISO 1947⁴⁴.

286 Most modern CNC machines have tapered interfaces that are made to AT3 or tighter for radial
 287 accuracy. For a taper of 10-16 mm length AT3 prescribes a maximum variances of 21'' (0.006 °) cone
 288 angle and 1.0-1.6 μm difference in diameter at L. This tolerance is especially important for interfaces
 289 which undergo higher rotational speeds and greater cutting forces⁴⁵. The tighter fit reduces
 290 vibration which has been shown to initiate fretting and affect the quality of the workpiece^{45,46}.

291 The manufacturing tolerances of taper angles in THR are not public knowledge although we can
 292 measure the range of samples used in this study. Using these and other published measurements of
 293 THR tapers we noted a maximum difference of around 0.05 ° in cone angle and 20 μm in diameter
 294 for a given taper design from the same manufacturer³⁷. The diameter may also have been
 295 underestimated due to a level of mechanical filtering from the 1.5 mm ruby tipped stylus. This would
 296 place clinical tapers closer to the tolerance grade of AT8 ($AT_\alpha = 0.057^\circ$, $L = 10\text{-}16 \mu\text{m}$), if not beyond.

297 No manufacturing process will ever be able to produce 'perfect' surfaces, especially not on complex
 298 geometrical shapes such as is present in THR. However, this study does suggest that more can be
 299 done in the way of increasing conformity at the interface in THR if tapered interfaces in CNC

300 machines can be routinely manufactured to AT3 tolerance grades or tighter. Future work that
301 involves mapping out the link between taper design and performance is aimed at providing evidence
302 for guidelines as to what tolerance grades are required, and a common understanding of what a
303 'good' taper interface in THR might look like.

304 4.1. Taper Angle Mismatch

305 The angular mismatch between the cones of female and male tapers (i.e. the difference in cone
306 angle between the female and male taper) affects engagement and the contact mechanics of the
307 taper junction³⁰. Assuming there was no mixing of female and male tapers between manufacturers,
308 the majority of possible head-stem couples presented a proximal angular mismatch (i.e. contact is
309 predicted to be concentrated towards the inner most point of the taper junction, away from the
310 taper opening) with an average value of $0.0231 \pm 0.008^\circ$ (Figure 11a). Proximal contacts are a design
311 feature for ceramic head couples to ensure most of the stress is experienced by the portion of the
312 head with the most material¹. However, 69 % of manufacturer C head-stem couples presented a
313 distal mismatch of $-0.0125 \pm 0.002^\circ$ (i.e. contact is predicted to be concentrated towards the
314 opening of the taper junction). In this case, male taper angles were consistent with other '12/14'
315 male tapers (MT7, Figure 4a) and female taper angles were smaller compared to other '12/14'
316 female tapers (FT5 and FT6 in Figure 5), suggesting this mismatch was governed by a smaller female
317 taper angle. The remaining 31 % presented an average mismatch of $0.008 \pm 0.002^\circ$, possibly an
318 attempt to achieve a matched contact for metal-on-polymer bearing couples. There was significant
319 difference between all manufacturer mismatch angles with a p-value < 0.05 between groups.

320 Despite mixing head and stems from different manufacturers being discouraged and classed as 'off-
321 label', one study by Tucker et al⁴⁷ reported that this does happen and resulted in a higher failure
322 rate. Figure 11b shows the distribution of angular mismatch for matched manufacturer couples
323 verses mixed manufacturer couples. On average the angular mismatch between the matched and
324 mixed manufacturer couples is similar. The mixed manufacturer couples demonstrated on average a
325 slightly larger proximal mismatch, greater distribution and range of possible angular mismatches
326 than the matched manufacturer couples. Depending on which two manufacturers are involved in the
327 mixed head-stem couple, angular mismatch will likely be increased but in very few cases this can be
328 decreased.

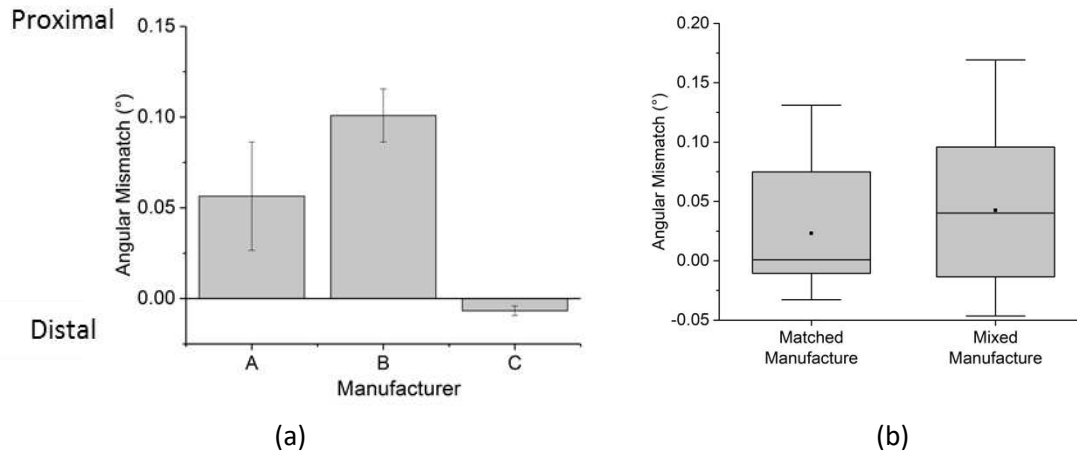


Figure 11 (a) Angular mismatch between cone angles of all matched manufacturer couples, separated by manufacturer. (b) Box plots that demonstrated the spread of angular mismatches for matched manufacturer couples vs mixed manufacturer couples (NB excluding MT8 and MT10), where the mean value has also been indicated by the block square point within each data set.

329 Some in-silico studies suggest that increasing conformity would reduce micro-motion at head-stem
 330 tapers and in-vitro studies at neck-stem adapters^{30,48}. Where micro-motion could increase by 3 μm
 331 for every 0.1° of angular mismatch. In comparison, this study found a maximum proximal angular
 332 mismatch of 0.131° and distal mismatch of -0.024°, suggesting an increase in micro-motion by 4 μm
 333 and 0.7 μm respectively, possibly increasing the amount degradation via fretting-corrosion. Other
 334 studies suggest that the level of angular mismatch present in the head-stem junction has an
 335 insignificant effect compared to other variables^{49,50}. Therefore, small manipulations of angular
 336 mismatch at the micro scale, like increasing the distal taper junction contact could create a seal to
 337 prevent fluid ingress, reducing fretting-corrosion as suggested by Witt et al.³⁹. However, it is
 338 unknown how the effect of other design parameters such as offset interact with mismatch and if this
 339 can be optimised with proximal and distal mismatches.

340 4.2. 'Roundness' and 'Straightness'

341 4.2.1. Male Tapers

342 Deviation from the idealised male taper geometry appeared to be linked to the flexural rigidity of
 343 the taper and lower stem geometry. For example the narrowest '10/12' taper (MT 8) presented the
 344 greatest out of 'roundness' demonstrated in Figure 8f. The pattern demonstrated noticeable ovality
 345 correlating with differences in the second moment of area of the lower stem geometry shown
 346 schematically in Figure 12. The major axis of the oval occurred at roughly $\theta = 0^\circ$ and $\theta = \pm 180^\circ$,
 347 which corresponds to the smaller second moment of area of the lower stem geometry. The smaller
 348 second moment of area allowing the male taper (workpiece) to flex away from the cutting tool
 349 allowing for material to lie above the ideal cone. Figure 8f also demonstrated an increase in
 350 deviation from the ideal cone towards the proximal end of the taper, consistent with simple

351 engineering beam bending theory principles. Conversely, the spigots (MT4 and MT5) did not
352 presented a difference in second moment of area and presented one of the smallest confidence
353 intervals in ideal taper angle (Figure 4) and a small variation in the quarter cone angles (Figure 6),
354 indicating good dimensional control during manufacture. MT7 presented the smallest variation in
355 taper angle and good dimensional control as shown by the surface deviation maps (Figure 8d). MT7
356 also presented the shortest ideal engagement length for better control during manufacture.

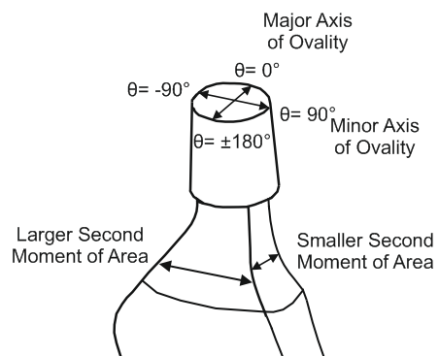


Figure 12 Schematic of how ovality relates to differences in second moments of area of the lower neck geometry.

357 Ovality was also seen in MT1, MT2, MT10 and MT11 (see Figure 8g, h, i and j). Where the non-
358 collared MT2 and MT11 presented ovality where the major axes occurred at $\theta = 0^\circ$ and $\theta = \pm 180^\circ$
359 corresponding to the smaller second moments of area, as was with MT 8. However, the collared
360 MT1 and MT 10 presented an oval pattern that was out of phase with the non-collared MT2, MT8
361 and MT11 by around 60° . One possible explanation for this is the collar altering the second
362 moments of area from what they would be if they were non-collared.

363 The elastic strain experienced during manufacturer is also controlled by the material properties of
364 the stem. One working hypothesis was that stems made with a relatively low elastic modulus such as
365 a titanium alloy would present greater variations in the form of out of 'roundness' and 'straightness'
366 compared to those made of a metal with a higher elastic modulus such as CoCrMo. However, results
367 did not consistently support this hypothesis and more measurements comparing stems with a
368 similar geometry made of different metals with a range of elastic moduli would be needed to
369 investigate this further.

370 Ovality could have significant implications on fretting-corrosion of the taper junction as it would
371 allow for stagnation of fluid and therefore increased crevice corrosion and possibly increase micro-
372 motion due to complex biomechanical loading²⁷. The effect of ovality was investigated using finite
373 elements models by Bitter et al⁵¹ that demonstrated increased micro-motion, contact pressures,
374 and wear compared to a 'perfect' fit. Other implications this study presented are those of volume
375 loss calculations post in-vitro assessment or from retrievals studies. Calculating the volume of
376 theoretical fluid that fills the space between the surface generated using the CMM surface maps and

377 maximum ideal cone (see Figure 13) presented a range of 0.5–5 mm³ for male tapers and 2.5–11
378 mm³ for female tapers. Material loss calculations of retrieved male tapers were within the range
379 0–0.8 mm³ and 0.41–25.89 mm³ for female tapers⁵². Material loss in the Racasan et al.⁵² study took
380 into account a threaded surface and any “barrelling” or “hogging” form. However, differences in
381 volume loss from other studies and theoretical mismatch in this study are of comparable scale.
382 Additionally, ovality in the male tapers and the triple peak pattern within the female tapers would
383 not be detected or taken into account on retrieval or damaged tapers.

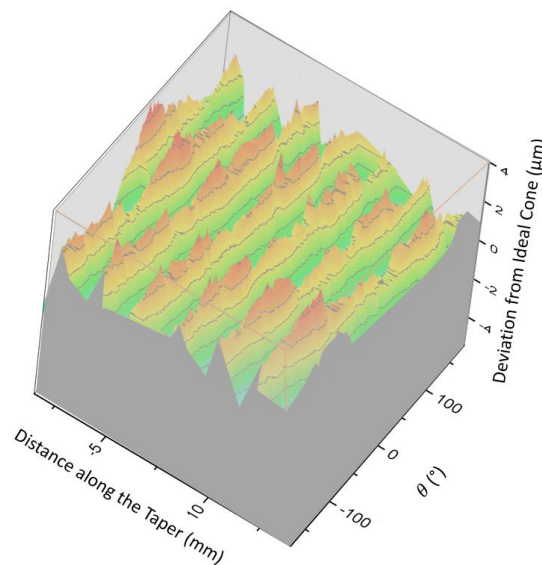


Figure 13 Schematic of theoretical volume of fluid that could fill the space between the actual taper surface and the maximum ideal cone.

384 4.2.2. Female Tapers

385 The female head tapers presented a similar level of out of roundness to the male stem tapers (see
386 Figure 5). Although much focus has been on the topography of the male taper and whether rough or
387 smooth male tapers have an implication on performance of the taper junction; local deviations from
388 the ideal cone of the female taper will have just as much implications in conformity between the two
389 components.

390 The four different types of female tapers that presented a third order harmonic (FT2, FT3, FT5 and
391 FT6) were all solid metal heads while the two remaining female tapers were either a hollow metal
392 head (i.e. assembled from a separate bearing surface and taper insert) (FT1) or ceramic (FT4). The
393 smallest cone angle deviation range was presented by the ceramic head (FT4) corresponding to the
394 smallest deviation range from the ideal cone possibly due to the sintering and grinding processes
395 involved in the manufacturer of ceramic heads. Although it is not quite clear where there third order
396 harmonic deviation pattern has come due to the spherical nature of the head, this is usually
397 attributed to distortion of the work piece by clamping or forces experienced during manufacture⁵³.

398 **5. Conclusions**

399 Conformity and engagement between the conical surfaces in a taper junction, a key design
400 parameter intended by Morse and is intuitively a performance determining factor. This study
401 suggested that engagement predicted by angular mismatch of the idealised geometries may be
402 insufficient. Rather, engagement is specific to a particular head and stem couple subject to both
403 their micro-scale variations superimposed on their macro-scale differences across the difference
404 length scale. Findings from this study raise the question of what a good taper junction looks like and
405 if these junctions can be optimised for specific head-stem couples in combination with any other
406 interacting design parameters such as offset i.e. does offset effect the performance of a distal
407 contact the same as a distal contact? The key findings from this study include:

- 408 • Tapers of the apparent same type (i.e. '12/14') presented different geometries
- 409 • Mixing of heads and stems from different manufacturers increased the variability in angular
410 mismatch
- 411 • Angular mismatches can be either proximal, distal or matched which could influence
412 fretting-corrosion of different head and stem designs in different ways i.e. material couples
413 and offsets
- 414 • Assuming an ideal geometry, deviation patterns were uniquely different between female
415 and male tapers, and appear to be linked to the manufacturing process
- 416 • Engagement is specific to a particular head and stem couple subject to both their micro-
417 scale variations superimposed on their macro-scale differences

418 **6. Acknowledgments**

419 The authors would like to thank MatOrtho LTD (UK) and the EPSRC Centre for Doctoral Training for
420 Integrated Tribology for their support.

421 **7. Declaration of Interest Statement**

422 Conflicts of Interest: None

423 Ethical Approval: Not required

424 Funding: This project was funded by MatOrtho LTD (UK) and the EPSRC Centre for Doctoral Training
425 for Integrated Tribology [Grant No. EPL01629X1].

426 **8. References**

- 427 1. Hernigou P, Queindec S, Flouzat Lachaniette CH. One hundred and fifty years of history of the
428 Morse taper: From Stephen A. Morse in 1864 to complications related to modularity in hip
429 arthroplasty. *Int Orthop*. 2013;37(10):2081-2088. doi:10.1007/s00264-013-1927-0

- 430 2. Collier JP, Mayor MB, Williams IR, Surprenant VA, Surprenant HP, Currier BH. The Tradeoffs
431 Associated With Modular Hip Prostheses. *Clin Orthop Relat Res Number*. 1995;311:91-101.
- 432 3. Traina F, De Fine M, Biondi F, Tassinari E, Galvani A, Toni A. The influence of the centre of
433 rotation on implant survival using a modular stem hip prosthesis. *Int Orthop*.
434 2009;33(6):1513-1518. doi:10.1007/s00264-008-0710-0
- 435 4. Goyal N, Ho H, Fricka KB, Engh CA. Do You Have to Remove a Corroded Femoral Stem? *J*
436 *Arthroplasty*. 2014;29(9):139-142. doi:10.1016/j.arth.2014.03.055
- 437 5. Garellick G, Kärrholm J, Rogmark C, Herberts P, Rolfson O. *Swedish Hip Arthroplasty Register -*
438 *Annual Report 2017.*; 2017.
- 439 6. National Joint Registry for England, Wales NI and I of M. 15th Annual Report 2018. *15th Annu*
440 *Rep*. 2017;1821(December 2017):218. doi:10.1038/nmat2505
- 441 7. Brown SA, Flemming CAC, Kawalec JS, et al. Fretting corrosion accelerates crevice corrosion
442 of modular hip tapers. *J Appl Biomater*. 1995;6(1):19-26. doi:10.1002/jab.770060104
- 443 8. Gilbert JL, Buckley CA, Jacobs JJ. In vivo corrosion of modular hip prosthesis components in
444 mixed and similar metal combinations. The effect of crevice, stress, motion, and alloy
445 coupling. *J Biomed Mater Res*. 1993;27(12):1533-1544.
- 446 9. Goldberg JR, Gilbert JL, Jacobs JJ, Bauer TW, Paprosky W, Leurgans S. A Multicenter Retrieval
447 Study of the Taper Interfaces of Modular Hip Prostheses. *Clin Orthop Relat Res*.
448 2002;401:149-161. doi:10.1097/00003086-200208000-00018
- 449 10. Cooper HJ, Della Valle CJ, Berger RA, et al. Corrosion at the head-neck taper as a cause for
450 adverse local tissue reactions after total hip arthroplasty. *J Bone Jt Surg - Ser A*. 2012;74-
451 A(18):1655-1661. doi:10.2106/JBJS.K.01352
- 452 11. Hall DJ, Pourzal R, Della Valle CJ, Galante JO, Jacobs JJ, Urban RM. Corrosion of Modular
453 Junctions in Femoral and Acetabular Components for Hip Arthroplasty and Its Local and
454 Systemic Effects. In: *Modularity and Tapers in Total Joint Replacement Devices*. 100 Barr
455 Harbor Drive, PO Box C700, West Conshohocken, PA 19428-2959: ASTM International;
456 2015:410-427. doi:10.1520/STP159120140134
- 457 12. Jennings JM, Dennis DA, Yang CC. Corrosion of the Head-neck Junction After Total Hip. *J Am*
458 *Acad Orthop Surg*. 2016;24(6):349-356. doi:10.5435/JAAOS-D-15-00111
- 459 13. Lindgren JU, Brismar BH, Wikstrom AC, Professor A. Adverse reaction to metal release from a
460 modular metal-on-polyethylene hip prosthesis. *J Bone Jt Surg Br*. 2011;9393(10):1427-1430.
461 doi:10.1302/0301-620X.93B10
- 462 14. Borden R, Pour AE, Murayama T, Blaha JD. Patient Outcomes Following Implantation of
463 Modular Neck Hip Prostheses in Primary Total Hip Arthroplasty. In: *Modularity and Tapers in*
464 *Total Joint Replacement Devices*. 100 Barr Harbor Drive, PO Box C700, West Conshohocken,
465 PA 19428-2959: ASTM International; 2015:17-25. doi:10.1520/STP159120140151
- 466 15. Morlock M, Bunte D, Gührs J, Bishop N. Corrosion of the Head-Stem Taper Junction—Are We
467 on the Verge of an Epidemic?: Review Article. *HSS J*. 2017;13:42-49. doi:10.1007/s11420-016-
468 9526-4
- 469 16. Waterson HB, Whitehouse MR, Greidanus N V., Garbus DS, Masri BA, Duncan CP. Revision for
470 adverse local tissue reaction following metal-on-polyethylene total hip arthroplasty is
471 associated with a high risk of early major complications. *Bone Joint J*. 2018;100-B(6):720-724.
472 doi:10.1302/0301-620X.100B6.BJJ-2017-1466.R1

- 473 17. Morlock MM. The Taper Disaster - How Could it Happen? *HIP Int.* 2015;25(4):339-346.
474 doi:10.5301/hipint.5000269
- 475 18. Ridon PE, Putman S, Migaud H, Berton C, Pasquier G, Girard J. Long-term comparative study
476 of large-diameter metal-on-metal bearings: Resurfacing versus total arthroplasty with large-
477 diameter Durom™ bearing. *Orthop Traumatol Surg Res.* 2019. doi:10.1016/j.otsr.2019.04.006
- 478 19. Higgs GB, MacDonald DW, Gilbert JL, et al. Does Taper Size Have an Effect on Taper Damage
479 in Retrieved Metal-on-Polyethylene Total Hip Devices? *J Arthroplasty.* 2016;31(9):277-281.
480 doi:10.1016/j.arth.2016.06.053
- 481 20. Bhalekar RM, Smith SL, Joyce TJ. Wear at the taper-trunnion junction of contemporary
482 ceramic-on-ceramic hips shown in a multistation hip simulator. *J Biomed Mater Res - Part B*
483 *Appl Biomater.* 2018;(November 2017):1-11. doi:10.1002/jbm.b.34213
- 484 21. Perrigo OE. *Modern American Lathe Practice.* New York: The Norman W. Henley Publishing
485 Co.; 1907.
- 486 22. Colvin FH. *Turning and Boring Tapers.* New York: The Derry-Collard Company; 1903.
- 487 23. BSI, ISO. BS 4500 Limits and Fits: Part 5. Specification for system of cone tolerances for
488 conical work pieces from C=1:3 to 1:500 and lengths from 6mm to 630mm. 1988.
- 489 24. Werner PH, Etema HB, Wit F, Morlock MM, Verheyen CCPM. Basic principles and uniform
490 terminology for the head-neck junction in hip replacement. *HIP Int.* 2015;25(2):115-119.
491 doi:10.5301/hipint.5000204
- 492 25. Bergmann G, Graichen F, Rohlmann A, et al. Realistic loads for testing hip implants. *Biomed*
493 *Mater Eng.* 2010;20:65-75. doi:10.3233/BME-2010-0616
- 494 26. Bishop NE, Hothan A, Morlock MM. High friction moments in large hard-on-hard hip
495 replacement bearings in conditions of poor lubrication. *J Orthop Res.* 2013;31(5):807-813.
496 doi:10.1002/jor.22255
- 497 27. Gilbert JL, Mali SA, Sivan S. Corrosion of Modular Tapers in Total Joint Replacements: A
498 Critical Assessment of Design, Materials, Surface Structure, Mechanics, Electrochemistry, and
499 Biology. In: *Modularity and Tapers in Total Joint Replacement Devices.* 100 Barr Harbor Drive,
500 PO Box C700, West Conshohocken, PA 19428-2959: ASTM International; 2015:192-223.
501 doi:10.1520/STP159120140135
- 502 28. Hothi HS, Eskelinen AP, Berber R, et al. Factors Associated With Trunnionosis in the Metal-on-
503 Metal Pinnacle Hip. *J Arthroplasty.* 2017;32(1):286-290. doi:10.1016/j.arth.2016.06.038
- 504 29. Whittaker RK, Hothi HS, Eskelinen A, Blunn GW, Skinner JA, Hart AJ. Variation in taper surface
505 roughness for a single design effects the wear rate in total hip arthroplasty. *J Orthop Res.*
506 2017;35:1784-1792. doi:10.1002/jor.23456
- 507 30. Donaldson FE, Coburn JC, Siegel KL. Total hip arthroplasty head-neck contact mechanics: A
508 stochastic investigation of key parameters. *J Biomech.* 2014;47:1634-1641.
509 doi:10.1016/j.jbiomech.2014.02.035
- 510 31. Panagiotidou A, Meswania J, Hua J, Muirhead-Allwood S, Hart A, Blunn G. Enhanced wear and
511 corrosion in modular tapers in total hip replacement is associated with the contact area and
512 surface topography. *J Orthop Res.* 2013;31(12):2032-2039. doi:10.1002/jor.22461
- 513 32. Brock TM, Sidaginamale R, Rushton S, et al. Shorter, rough trunnion surfaces are associated
514 with higher taper wear rates than longer, smooth trunnion surfaces in a contemporary large
515 head metal-on-metal total hip arthroplasty system. *J Orthop Res.* 2015;33(12):1868-1874.

516 doi:10.1002/jor.22970

517 33. Kao YYJ, Koch CN, Wright TM, Padgett DE. Flexural Rigidity, Taper Angle, and Contact Length
518 Affect Fretting of the Femoral Stem Trunnion in Total Hip Arthroplasty. *J Arthroplasty*.
519 2016;31(9):254-258. doi:10.1016/j.arth.2016.02.079

520 34. Jauch-Matt SY, Miles AW, Gill HS. Effect of trunnion roughness and length on the modular
521 taper junction strength under typical intraoperative assembly forces. *Med Eng Phys*.
522 2017;39:94-101. doi:10.1016/j.medengphy.2016.11.001

523 35. Woon CY, Wach A, Wright TM, Padgett DE. Taper Design, Head Material, and Manufacturer
524 Affect the Onset of Fretting Under Simulated Corrosion Conditions. *J Arthroplasty*. November
525 2019. doi:10.1016/j.arth.2019.11.005

526 36. Hothi HS, Whittaker RK, Meswania JM, Blunn GW, Skinner JA, Hart AJ. Influence of stem type
527 on material loss at the metal-on-metal pinnacle taper junction. *Proc Inst Mech Eng Part H J*
528 *Eng Med*. 2015;229(1):91-97. doi:10.1177/0954411914567931

529 37. Mueller U, Braun S, Schroeder S, Sonntag R, Kretzer JP. Same Same but Different? 12/14 Stem
530 and Head Tapers in Total Hip Arthroplasty. *J Arthroplasty*. 2017;32:3191-3199.
531 doi:10.1016/j.arth.2017.04.027

532 38. Munir S, Walter WL, Walsh WR. Variations in the trunnion surface topography between
533 different commercially available hip replacement stems. *J Orthop Res*. 2015;33(1):98-105.
534 doi:10.1002/jor.22741

535 39. Witt F, Gührs J, Morlock MM, Bishop NE. Quantification of the contact area at the head-stem
536 taper interface of modular hip prostheses. *PLoS One*. 2015;10(8):1-15.
537 doi:10.1371/journal.pone.0135517

538 40. BSI. ISO 14242-2 Implants for surgery - Wear of total hip joint prostheses - Part 2 : Methods
539 of measurement. *BSI*. 2000;14242(2).

540 41. Nassif NA, Nawabi DH, Stoner K, Elpers M, Wright T, Padgett DE. Taper Design Affects Failure
541 of Large-head Metal-on-metal Total Hip Replacements. *Clin Orthop Relat Res*.
542 2014;472(2):564-571. doi:10.1007/s11999-013-3115-3

543 42. Ouellette ES, Shenoy AA, Gilbert JL. The seating mechanics of head-neck modular tapers in
544 vitro: Load-displacement measurements, moisture, and rate effects. *J Orthop Res*.
545 2018;36(4):1164-1172. doi:10.1002/jor.23725

546 43. Morlock MM, Dickinson EC, Günther KP, Bünte D, Polster V. Head Taper Corrosion Causing
547 Head Bottoming Out and Consecutive Gross Stem Taper Failure in Total Hip Arthroplasty. *J*
548 *Arthroplasty*. 2018;33(11):3581-3590. doi:10.1016/j.arth.2018.07.017

549 44. ISO1947-1973. BS 4500 Limits and Fits: Part 5. Specification for system of cone tolerances for
550 conical work pieces from C=1:3 to 1:500 and lengths from 6mm to 630mm. 1988.

551 45. David A. Stephenson JSA. Toolholders and Workholders. In: *Metal Cutting Theory and*
552 *Practice*. 3rd ed. New York: Taylor & Francis Group; 2016:280-332.

553 46. Rivin EI. Advanced 7/24 taper toolholder/spindle interfaces for high-speed CNC machine
554 tools. *SAE Tech Pap*. 1998;(724). doi:10.4271/981866

555 47. Tucker K, Pickford M, Newell C, Howard P, Hunt LP, Blom AW. Mixing of components from
556 different manufacturers in total hip arthroplasty: Prevalence and comparative outcomes.
557 *Acta Orthop*. 2015;86(6):671-677. doi:10.3109/17453674.2015.1074483

- 558 48. Haschke H, Jauch-Matt SY, Sellenschloh K, Huber G, Morlock MM. Assembly force and taper
559 angle difference influence the relative motion at the stem-neck interface of bi-modular hip
560 prostheses. *Proc Inst Mech Eng Part H J Eng Med*. 2016;230(7):690-699.
561 doi:10.1177/0954411916648717
- 562 49. Kocagöz SB, Underwood RJ, Sivan S, et al. Does taper angle clearance influence fretting and
563 corrosion damage at the head-stem interface? A matched cohort retrieval study. *Semin*
564 *Arthroplasty*. 2013;24(4):246-254. doi:10.1053/j.sart.2014.01.002
- 565 50. Ouellette ES, Mali SA, Kim J, Grostefon J, Gilbert JL. Design, Material, and Seating Load Effects
566 on In Vitro Fretting Corrosion Performance of Modular Head-Neck Tapers. *J Arthroplasty*.
567 2019;34(5):991-1002. doi:10.1016/j.arth.2019.01.043
- 568 51. Bitter T, Khan I, Marriott T, Lovelady E, Verdonschot N, Janssen D. The effects of
569 manufacturing tolerances and assembly force on the volumetric wear at the taper junction in
570 modular total hip arthroplasty. *Comput Methods Biomech Biomed Engin*. 2019;22(13):1061-
571 1072. doi:10.1080/10255842.2019.1627524
- 572 52. Racasan R, Bills P, Blunt L, Hart A, Skinner J. Method for Characterization of Material Loss
573 from Modular Head-Stem Taper Surfaces of Hip Replacement Devices. In: *Modularity and*
574 *Tapers in Total Joint Replacement Devices*. 100 Barr Harbor Drive, PO Box C700, West
575 Conshohocken, PA 19428-2959: ASTM International; 2015:132-146.
576 doi:10.1520/STP159120140139
- 577 53. Taylor Hobson. *A Guide to Roundness and Surface Texture - Measurement and Parameters*.
578 1st ed. Leicester: Taylor Hobson; 2017. www.taylor-hobson.com.
- 579